

ELM Crash with Nonlinear Toroidally Axisymmetric Flow and Field

H. Seto¹, X.Q. Xu², B.D. Dudson³ and M. Yagi¹

¹QST, ²LLNL, ³U. York

OUTLINE

1. Backgrounds and Motivations
2. Numerical Schemes for $n=0$ flow/field in BOUT++ framework
3. Role of $n=0$ flow/field in ELM crash
4. Summary and Future Works

This work was supported by JSPS KAKENHI Grant No.16K18342 and was also performed under the auspices of the U.S. Department of Energy by Lawrence Livermore National Laboratory under Contract No. DE-AC52-07NA27344. Computations were carried out on JFRS-1 supercomputer at IFERC-CSC, ITO-A supercomputer at Kyushu University and ICE-X supercomputer at JAEA.

Backgrounds

It is one of key issues for ITER and DEMO to understand nonlinear dynamics in ELMs and their energy loss process

- JOREK code (5-f RMHD w/o two-fluid effect)[1,2] reveals that
 - ✓ Convective cell generated by mode couplings among low- n ~ middle- n ballooning modes shears density filaments
 - ➔ $n=0$ flow can have considerable impact on ELM process
- BOUT++ code[3] has not solved $n=0$ component of vorticity Eq. and Ohm's law in ELM simulations due to numerical problems
 - ✓ Net nonlinear $n=0$ flow is set to zero
 - ✓ Nonlinear $n=0$ field is assumed to be negligibly small
 - ➔ ELMs with $n=0$ flow/field have been future work so far

Motivations

It is challenging for MHD code using flux surface coordinate to handle high- n mode while it can handle low- \sim middle- n consistently

- **Flux-surface-aligned grid** requires a huge number of poloidal grids for describing high- n modes
- BOUT++ employs **field-aligned grid** as well as **flux-surface-aligned grid** for describing high- n modes efficiently
 - ➔ Improving BOUT++ is one of solutions to simulate ELMs with $n=0$ flow/field driven by middle- $n \sim$ high- n ballooning modes

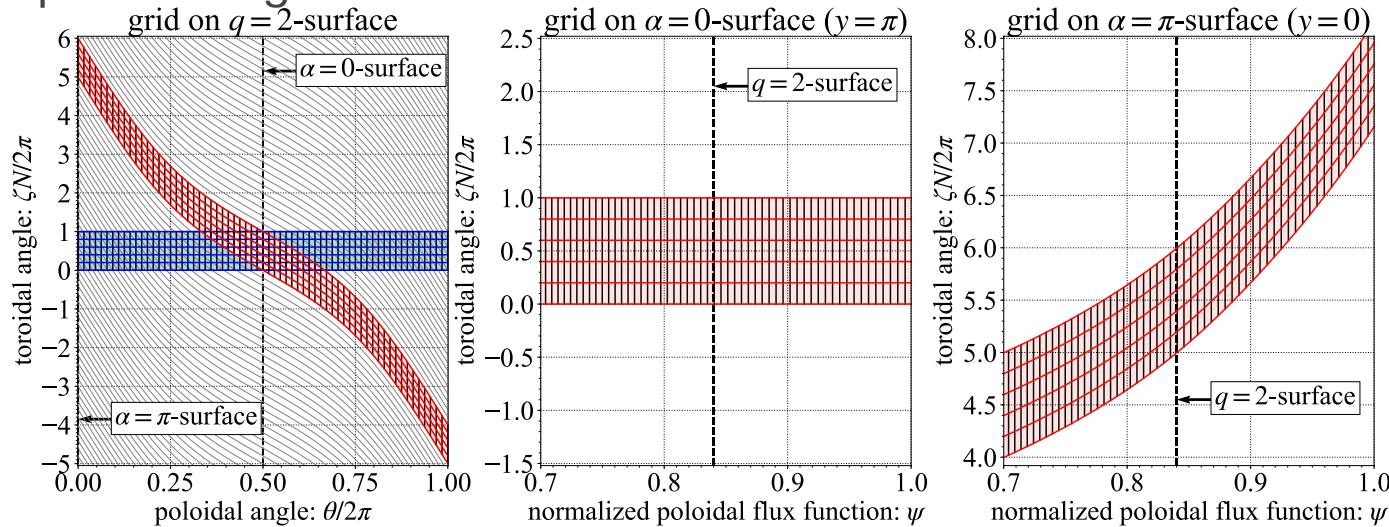
Main topics of this talk

- A numerical scheme designed for multi-helicity ELM simulation with $n=0$ flow/field is demonstrated
- Role of $n=0$ flow/field in ELM crash process is investigated with two ion diamagnetism models (used in JOREK and BOUT++)

1. Background and Motivations
2. Numerical Scheme for $n=0$ flow/field Driven by high- n Modes
 - 1) Coordinate Systems in BOUT++
 - 2) Numerical Problems and Their Remedies
 - 3) Physics Models and Simulation Setup
 - 4) Validation Study of Presenting Scheme
3. Role of $n=0$ flow/field in ELM crash
4. Summary and Future Works

Coordinate Systems in BOUT++: 1/2

Computational grid of 1/5th annular torus in flux-surface coordinate (cbm18_dens4 [4])



safety factor q is negative definite so that $-q$ is used as surface label for readability

[4]: N.M. Ferraro+ PoP2010

Quasi-ballooning coordinate system in BOUT++ consists of

- Orthogonal flux coordinate system (ψ, θ, ζ)
 - ✓ Huge number of poloidal grids are required for high- n modes
- Field-aligned coordinate system (x, y, z)
 - ✓ Parallel derivatives can be efficiently evaluated
 - ✓ Integrated magnetic shear I results in secular cell deformation

$$x = \psi - \psi_{\text{sep}}, \quad y = \theta, \quad z = \zeta - \alpha, \quad \alpha = \int_{\theta_0}^{\theta} \nu d\theta, \quad \nu = \frac{B_t h_\theta}{B_p R}, \quad q = \frac{1}{2\pi} \oint \nu d\theta, \quad I = \frac{\partial \alpha}{\partial \psi}$$

$$\mathbf{e}_x = \mathbf{e}_\psi + I \mathbf{e}_\zeta, \quad \mathbf{e}_y = \mathbf{e}_\theta + \nu \mathbf{e}_\zeta, \quad \mathbf{e}_z = \mathbf{e}_\zeta, \quad \mathbf{e}^x = \mathbf{e}^\psi, \quad \mathbf{e}^y = \mathbf{e}^\theta, \quad \mathbf{e}^z = -I \mathbf{e}^\psi - \nu \mathbf{e}^\theta + \mathbf{e}^\zeta$$

Coordinate Systems in BOUT++: 2/2

Quasi-ballooning coordinate system (ψ, y, z) : $(\psi, \theta, \zeta) + (x, y, z)$

- The following schemes are employed to remove cell deformation

✓ Shifted radial derivative

$$\frac{\partial}{\partial x} f(x, y, z) = \frac{\partial}{\partial \psi} f(\psi, \theta, \zeta) + I \frac{\partial}{\partial z} f(x, y, z)$$

✓ Shifted metrics (basis)

$$\begin{aligned} e_u &= e_x - I e_z, & e_v &= e_y, & e_w &= e_z, \\ e^u &= e^x, & e^v &= e^y, & e^w &= e^z + I e^x, \end{aligned}$$

- Differential operators are now written in I -free forms

✓ e.g. Divergence of vector A

$$\begin{aligned} \nabla \cdot \mathbf{A} &= \frac{1}{J} \frac{\partial}{\partial x} (JA^x) + \frac{1}{J} \frac{\partial}{\partial y} (JA^y) + \frac{1}{J} \frac{\partial}{\partial z} (JA^z) \\ &= \frac{1}{J} \left(\frac{\partial}{\partial \psi} + I \frac{\partial}{\partial z} \right) (JA^u) + \frac{1}{J} \frac{\partial}{\partial y} (JA^v) + \frac{1}{J} \frac{\partial}{\partial z} [J(A^w - IA^u)] \\ &= \frac{1}{J} \frac{\partial}{\partial \psi} (JA^u) + \frac{1}{J} \frac{\partial}{\partial y} (JA^v) + \frac{1}{J} \frac{\partial}{\partial z} (JA^w) \end{aligned}$$

❖ Differential operators are expressed by differentials in 2D (ψ, ζ) - and 2D (y, z) -plane

Poisson solver in quasi-ballooning coordinates (ψ, y, n) however cannot be implemented as a 2D-boundary problem in (ψ, y) for each toroidal mode number n

- **Poisson solver:** $d\nabla_{\perp}^2 f + \frac{1}{c} \nabla c \cdot \nabla_{\perp} f + af = b$

Original scheme

✓ Flute-ordered 1D-Helmholtz Eq. solver for all toroidal modes

$$dg^{uu} \frac{\partial^2 F}{\partial \psi^2} + \left(dG^u + \frac{g^{uu}}{c} \frac{\partial c}{\partial \psi} \right) \frac{\partial F}{\partial \psi} + (a - dn^2 g^{ww} + indG^w) F = \mathcal{F} \{b\} e^{-in\alpha}$$

➔ This solver cannot reproduce poloidal structure for $n=0$



Presenting scheme

✓ Flute-ordered 1D-Helmholtz Eq. solver for resonant modes

✓ 2D-Helmholtz Eq. solver for $n=0$ mode ($e_y = e_{\theta}$ for $n=0$ mode)[5]

$$dg^{uu} \frac{\partial^2 \bar{f}}{\partial x^2} + \left(dG^u + \frac{g^{uu}}{c} \frac{\partial c}{\partial x} \right) \frac{\partial \bar{f}}{\partial x} + d \left(g^{vv} - \frac{1}{g_{vv}} \right) \frac{\partial^2 \bar{f}}{\partial y^2} + \frac{d}{J} \frac{\partial}{\partial y} \left[J \left(g^{vv} - \frac{1}{g_{vv}} \right) \right] \frac{\partial \bar{f}}{\partial y} + a\bar{f} = \bar{b}$$

$$F(\psi, \theta, n) = \mathcal{F} \{f(x, y, z)\} e^{-in\alpha}, \quad \bar{f}(x, y) : n=0 \text{ component of 3D field } f(x, y, z)$$

- **Poisson bracket:** $[f, g] = \frac{\mathbf{b} \times \nabla f \cdot \nabla g}{B}$

Original scheme

✓ Discretized with 3rd order WENO scheme

$$[f, g] = \frac{\mathbf{b} \times \nabla f \cdot \nabla g}{B} = \mathbf{V} \cdot \nabla g = V^u \frac{\partial g}{\partial \psi} + V^v \frac{\partial g}{\partial y} + V^w \frac{\partial g}{\partial z}$$

- ❖ **Using Up-winding scheme in core region gives spectrum contamination** in case of multi-helicity simulation due to numerical nonlinearity driven by time variation of stencils



Presenting scheme

✓ Discretized with symmetric scheme: FFT (z) + 4th central (ψ, y)

$$[f, g] = \frac{\mathbf{b} \times \nabla f \cdot \nabla g}{B} = \frac{\partial f}{\partial z} \frac{\partial g}{\partial \psi} - \frac{\partial f}{\partial \psi} \frac{\partial g}{\partial z} + \frac{g_{vw}}{g_{vw}} \left(\frac{\partial f}{\partial \psi} \frac{\partial \bar{g}}{\partial y} - \frac{\partial \bar{f}}{\partial y} \frac{\partial g}{\partial \psi} \right)$$

- ❖ **3D conservative scheme (e.g. Morinishi-scheme) is not straightforwardly available** due to non-commutative property of y - and ψ - derivative (remained as a future work)

- **Hazeltine-Meiss (HM) 4-field P-B model: $(U_1, P_1, A_{||1}, v_{||1})$**
Perp. flow expressed with electrostatic potential like JOREK [6]
- **Chang-Callen (CC) 4-field P-B model: $(W_1, P_1, A_{||1}, v_{||1})$**
Perp. flow expressed with generalized flow potential like BOUT++ [7]

$$\begin{aligned} \frac{\partial U_1}{\partial t} &= - [\phi_1, U_1] - \nabla_{||} J_{||1} + B_0 \left[A_{||1}, \frac{J_{||0}}{B_0} \right] + \mathcal{K}(p_1) \\ &\quad - \mathcal{G}(\phi_1, p) + \mu_{||} \partial_{||0}^2 U_1 + \mu_{\perp} \nabla_{\perp}^2 U_1 \\ \frac{\partial p_1}{\partial t} &= - [\phi_1, p] - \beta_* [2\mathcal{K}(\phi_1) + \nabla_{||} (v_{||1} + 2\delta_e J_{||1})] \\ &\quad + \chi_{||} \partial_{||0}^2 p_1 + \chi_{\perp} \nabla_{\perp}^2 p_1 \\ \frac{\partial A_{||1}}{\partial t} &= - \partial_{||} (\phi_1 - \delta_e p_1) - \delta_e [A_{||1}, p_0] + \eta J_{||1} - \lambda \nabla_{\perp}^2 J_{||1} \\ \frac{\partial v_{||1}}{\partial t} &= - [\phi_1, v_{||1}] - \frac{1}{2} (\partial_{||} p_1 - [A_{||1}, p_0]) + \nu_{||} \nabla_{\perp}^2 v_{||1} \\ U &= \nabla \cdot \left(\frac{\nabla_{\perp} \phi}{B_0^2} \right), \quad J_1 = \nabla_{\perp}^2 A_{||1} \quad \delta_i = \delta_e = \frac{d_i}{4} \end{aligned}$$

$$\begin{aligned} \frac{\partial W_1}{\partial t} &= - [F, W_1] - [F_1, W_0] - \nabla_{||} J_{||1} + B_0 \left[A_{||1}, \frac{J_{||0}}{B_0} \right] + \mathcal{K}(p_1) \\ &\quad + \mathcal{G}(p, F_1) + \mathcal{G}(p_1, F_0) + \mu_{||} \partial_{||0}^2 W_1 + \mu_{\perp} \nabla_{\perp}^2 W_1 \\ \frac{\partial p_1}{\partial t} &= - [\phi_1, p] - \beta_* [2\mathcal{K}(\phi_1) + \nabla_{||} (v_{||1} + d_i J_{||1})] \\ &\quad + \chi_{||} \partial_{||0}^2 p_1 + \chi_{\perp} \nabla_{\perp}^2 p_1 \\ \frac{\partial A_{||1}}{\partial t} &= - \partial_{||} (\phi_1 - \delta_e p_1) - \delta_e [A_{||1}, p_0] + \eta J_{||1} - \lambda \nabla_{\perp}^2 J_{||1} \\ \frac{\partial v_{||1}}{\partial t} &= - [\phi_1, v_{||1}] - \frac{1}{2} (\partial_{||} p_1 - [A_{||1}, p_0]) + \nu_{||} \nabla_{\perp}^2 v_{||1} \\ W &= \nabla \cdot \left(\frac{\nabla_{\perp} F}{B_0^2} \right), \quad F = \phi + \delta_i p, \quad J_1 = \nabla_{\perp}^2 A_{||1} \quad \delta_i = \delta_e = \frac{d_i}{4} \end{aligned}$$

$$\begin{aligned} \nabla_{||} f &= B_0 \partial_{||} \left(\frac{f}{B_0} \right), \quad \partial_{||} f = \mathbf{b} \cdot \nabla f = \partial_{||0} f - [A_{||1}, f], \quad \partial_{||0} f = \mathbf{b}_0 \cdot \nabla f, \quad [f, g] = \frac{\mathbf{b}_0 \times \nabla_{\perp} f \cdot \nabla_{\perp} g}{B_0} \quad f = f_0 + f_1 \\ \mathcal{G}(f, g) &= \frac{\delta_i}{2} \left\{ \left[f, \nabla \cdot \left(\frac{\nabla_{\perp} g}{B_0} \right) \right] + \left[g, \nabla \cdot \left(\frac{\nabla_{\perp} f}{B_0} \right) \right] + \nabla \cdot \left(\frac{\nabla_{\perp} [f, g]}{B_0} \right) \right\}, \quad \mathcal{K}(f) = \mathbf{b}_0 \times \boldsymbol{\kappa}_0 \cdot \nabla f, \quad \nabla_{\perp} f = (\nabla - \mathbf{b}_0 \partial_{||0}) f \end{aligned}$$

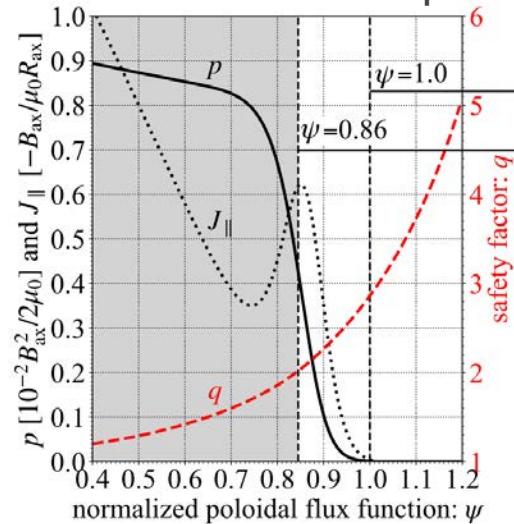
- **Hazeltine-Meiss (HM) 4-field P-B model: $(U_1, P_1, A_{\parallel 1}, v_{\parallel 1})$**
Perp. flow expressed with electrostatic potential like JOEREK [6]
- **Chang-Callen (CC) 4-field P-B model: $(W_1, P_1, A_{\parallel 1}, v_{\parallel 1})$**
Perp. flow expressed with generalized flow potential like BOUT++ [7]

$$\begin{aligned}
 \frac{\partial U_1}{\partial t} &= -[\phi_1, U_1] - \nabla_{\parallel} J_{\parallel 1} + B_0 \left[A_{\parallel 1}, \frac{J_{\parallel 0}}{B_0} \right] + \mathcal{K}(p_1) \\
 &\quad - \mathcal{G}(\phi_1, p) + \mu_{\parallel} \partial_{\parallel 0}^2 U_1 + \mu_{\perp} \nabla_{\perp}^2 U_1 \\
 \frac{\partial p_1}{\partial t} &= -[\phi_1, p] - \beta_* [2\mathcal{K}(\phi_1) + \nabla_{\parallel} (v_{\parallel 1} + 2\delta_e J_{\parallel 1})] \\
 &\quad + \chi_{\parallel} \partial_{\parallel 0}^2 p_1 + \chi_{\perp} \nabla_{\perp}^2 p_1 \\
 \frac{\partial A_{\parallel 1}}{\partial t} &= -\partial_{\parallel} (\phi_1 - \delta_e p_1) - \delta_e [A_{\parallel 1}, p_0] + \eta J_{\parallel 1} - \lambda \nabla_{\perp}^2 J_{\parallel 1} \\
 \frac{\partial v_{\parallel 1}}{\partial t} &= -[\phi_1, v_{\parallel 1}] - \frac{1}{2} (\partial_{\parallel} p_1 - [A_{\parallel 1}, p_0]) + \nu_{\parallel} \nabla_{\perp}^2 v_{\parallel 1} \\
 U &= \nabla \cdot \left(\frac{\nabla_{\perp} \phi}{B_0^2} \right), \quad J_1 = \nabla_{\perp}^2 A_{\parallel 1} \quad \delta_i = \delta_e = \frac{d_i}{4}
 \end{aligned}$$

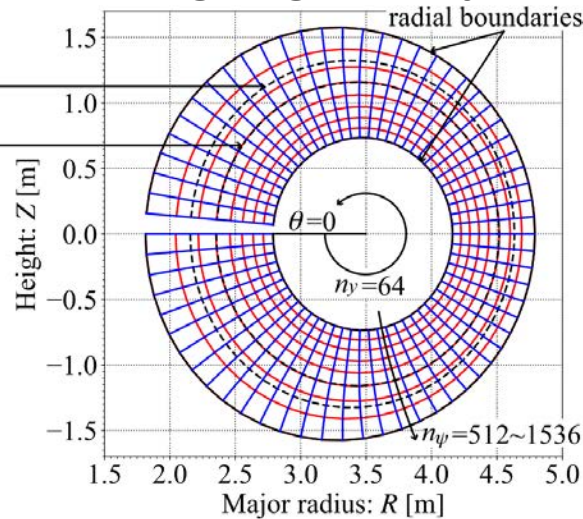
$$\begin{aligned}
 \frac{\partial W_1}{\partial t} &= -[F, W_1] - [F_1, W_0] - \nabla_{\parallel} J_{\parallel 1} + B_0 \left[A_{\parallel 1}, \frac{J_{\parallel 0}}{B_0} \right] + \mathcal{K}(p_1) \\
 &\quad + \mathcal{G}(p, F_1) + \mathcal{G}(p_1, F_0) + \mu_{\parallel} \partial_{\parallel 0}^2 W_1 + \mu_{\perp} \nabla_{\perp}^2 W_1 \\
 \frac{\partial p_1}{\partial t} &= -[\phi_1, p] - \beta_* [2\mathcal{K}(\phi_1) + \nabla_{\parallel} (v_{\parallel 1} + d_i J_{\parallel 1})] \\
 &\quad + \chi_{\parallel} \partial_{\parallel 0}^2 p_1 + \chi_{\perp} \nabla_{\perp}^2 p_1 \\
 \frac{\partial A_{\parallel 1}}{\partial t} &= -\partial_{\parallel} (\phi_1 - \delta_e p_1) - \delta_e [A_{\parallel 1}, p_0] + \eta J_{\parallel 1} - \lambda \nabla_{\perp}^2 J_{\parallel 1} \\
 \frac{\partial v_{\parallel 1}}{\partial t} &= -[\phi_1, v_{\parallel 1}] - \frac{1}{2} (\partial_{\parallel} p_1 - [A_{\parallel 1}, p_0]) + \nu_{\parallel} \nabla_{\perp}^2 v_{\parallel 1} \\
 W &= \nabla \cdot \left(\frac{\nabla_{\perp} F}{B_0^2} \right), \quad F = \phi + \delta_i p, \quad J_1 = \nabla_{\perp}^2 A_{\parallel 1} \quad \delta_i = \delta_e = \frac{d_i}{4}
 \end{aligned}$$

- ✓ Only lowest FLR effects are taken in ion gyro-viscous models
- ✓ Both models also include electron drift wave, flow compression (GAM, ion acoustic wave), resistivity and hyper-resistivity

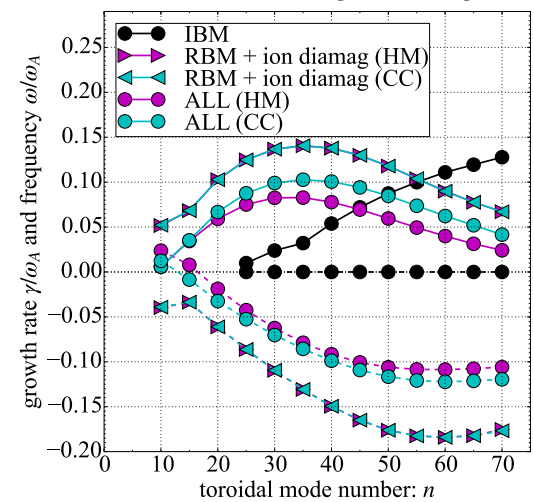
profiles on outer mid-plane



grid geometry



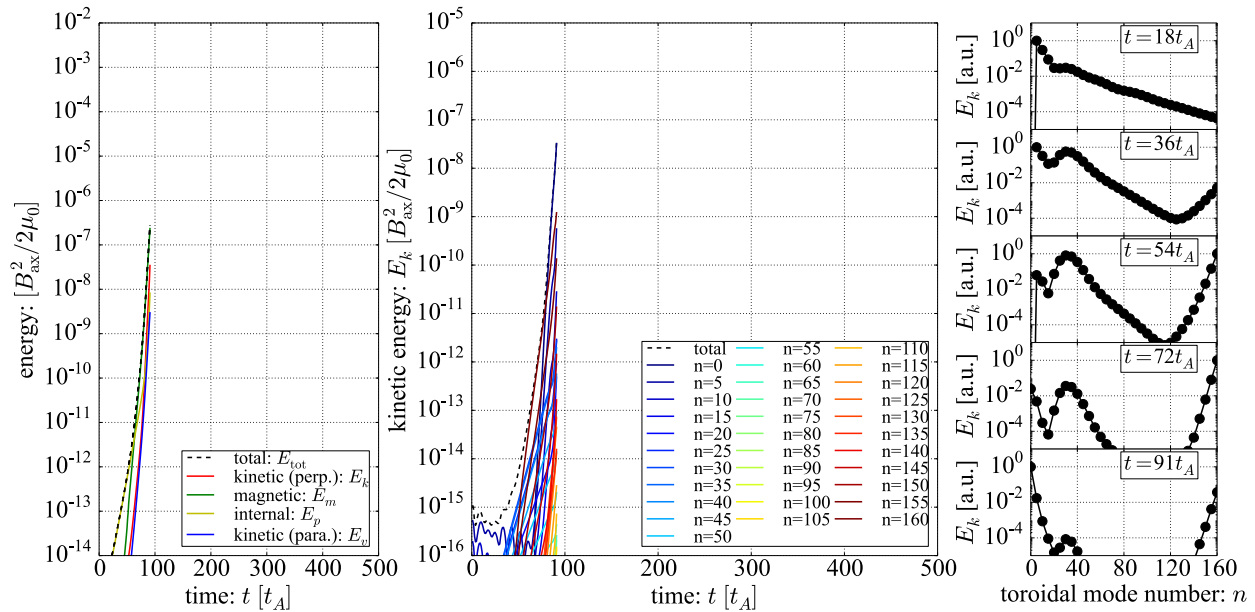
linear stability analysis



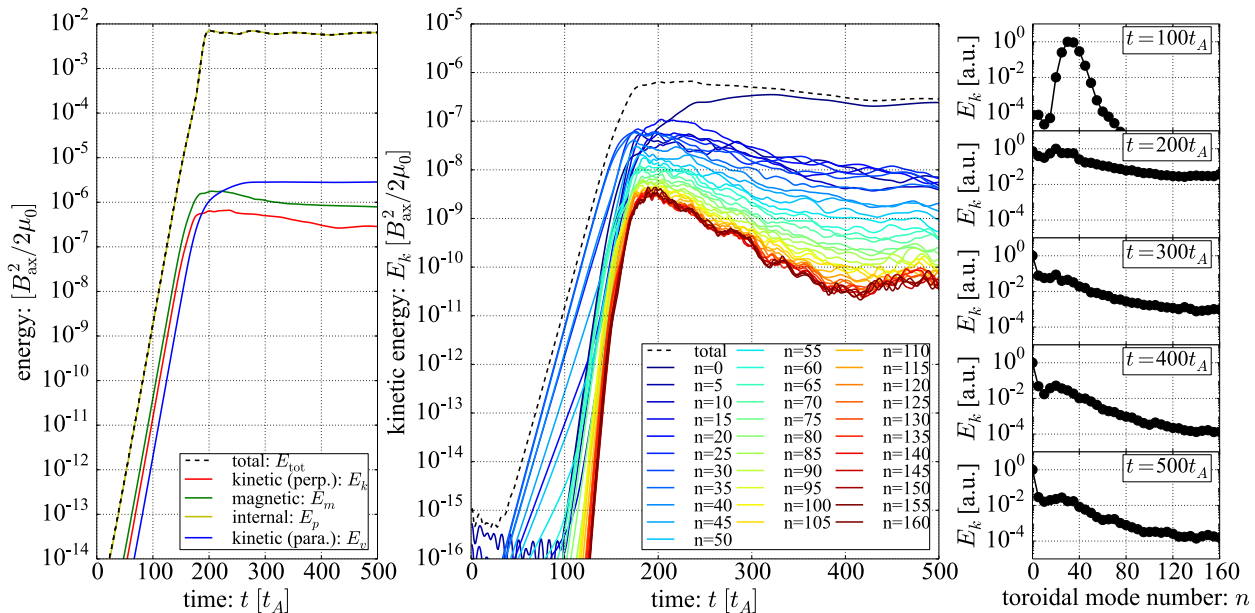
- Energy loss defined by energy released from the shaded region
- Resolution: $n_x=1536$, $n_y=64$, $n_z=128$ for 1/5th annular torus
- No sink/ source/ equilibrium flows/ equilibrium E_r models
- **CC model** is more unstable than **HM model** in case with the following parameter set
 - ✓ Normalizations: $n_{i0} = 10^{19} \text{ [m}^{-3}\text{]}$ (flat profile), $R_{\text{ax}} = 3.5 \text{ [m]}$, $B_{\text{ax}} = 2.0 \text{ [T]}$, $t_A = 3.6 \times 10^{-7} \text{ [s]}$
 - ✓ Dissipations: $\mu_{\parallel} = \chi_{\parallel} = 10^{-1}$, $\mu_{\perp} = \chi_{\perp} = \nu_{\perp} = 10^{-7}$, $\eta = 10^{-8}$, $\lambda = 10^{-12}$

Spectrum Contamination by WENO (HM)

- WENO bracket
 - ✓ Inverse energy cascade from **high- n driven nonlinearity by time variation of stencils**

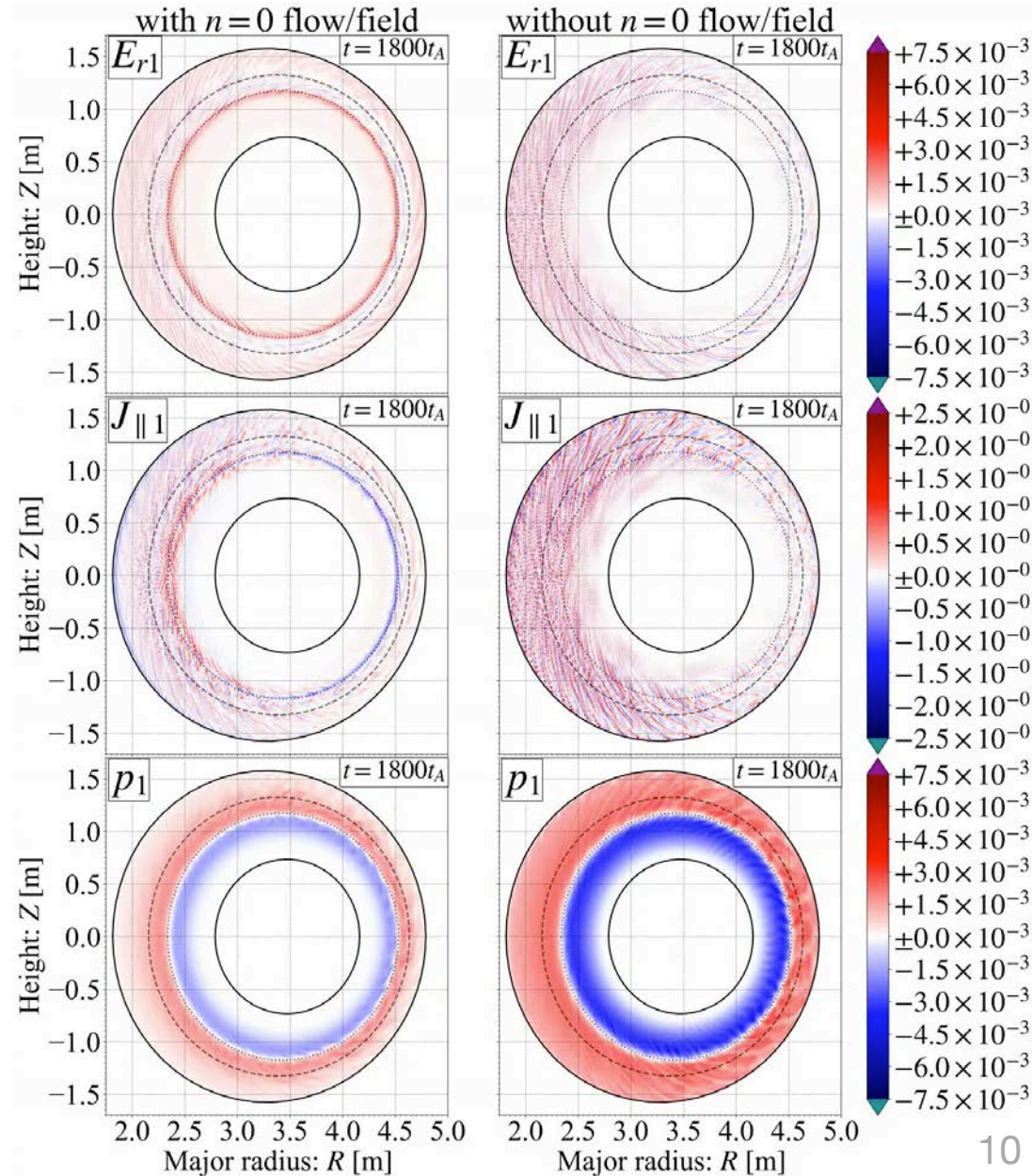


- Pseudo-spectrum bracket
 - ✓ Good energy conservation
 - ✓ Energy cascade and inverse energy cascade from $n=15\sim 65$



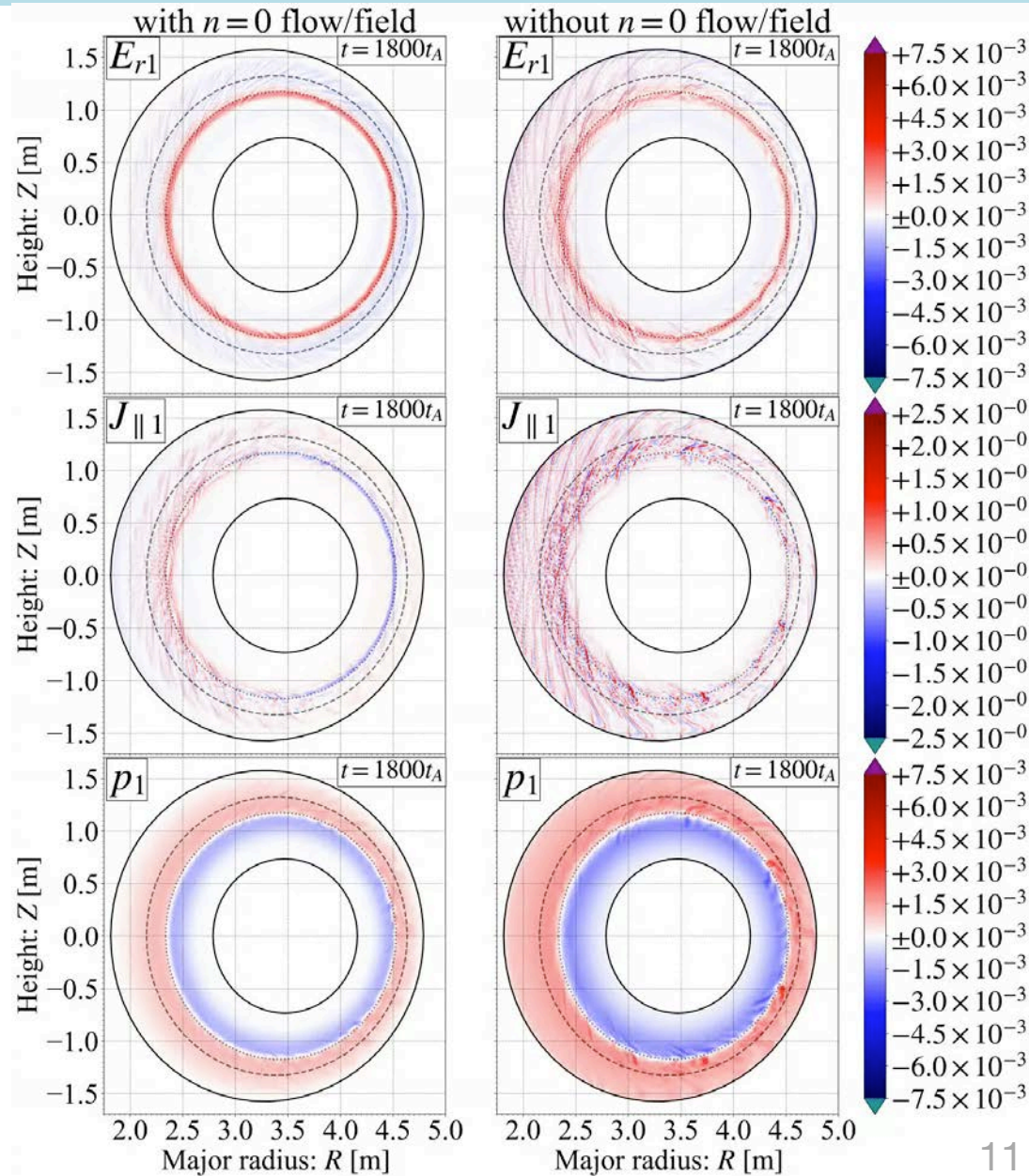
1. Backgrounds and Motivations
2. Numerical Scheme for $n=0$ flow/field Driven by high- n Modes
3. Role of $n=0$ flow/field in ELM crash
 - 1) E_{r1} , $J_{//1}$, P_1 at $\zeta=0$ w/ and w/o $n=0$ flow/field (movie)
 - 2) Impact of $n=0$ flow/field on Energy Loss Level
 - 3) Spatio-Temporal Analysis on Zonal Mode
 - 4) Energy Transfer Analysis of $n=0$ Kinetic Energy
4. Summary and Future Works

- E_r and J_{\parallel} filaments are obtained at pedestal crash in both cases
- $n=0$ global structures are then generated in E_r and J_{\parallel} profiles only in case w/ $n=0$ flow/field
- Convective cell shears pressure filaments and reduces their radial propagation in case w/ $n=0$ flow/field

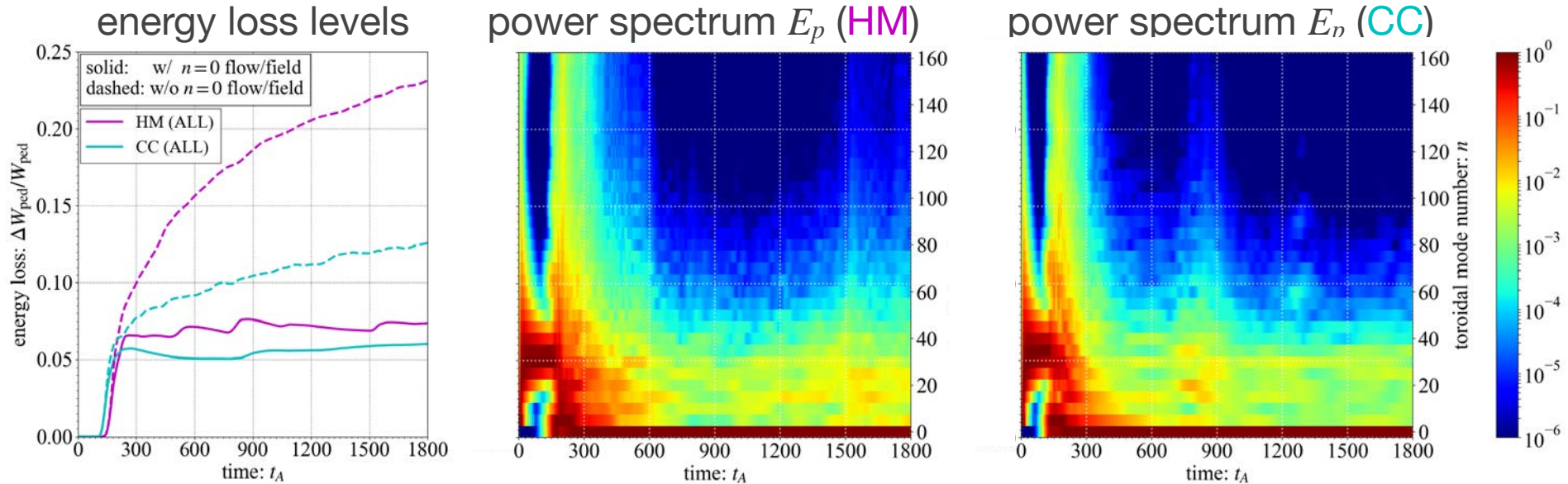


Differences from HM case are followings

- $n=0 E_r$ is sheared more strongly than that in HM model in case w/ $n=0$ flow/field
- $n=0$ global structure is partially generated in E_r profile even in case w/o $n=0$ flow/field via constraint $F_1 = \phi_1 + \delta_i p_1 = 0$



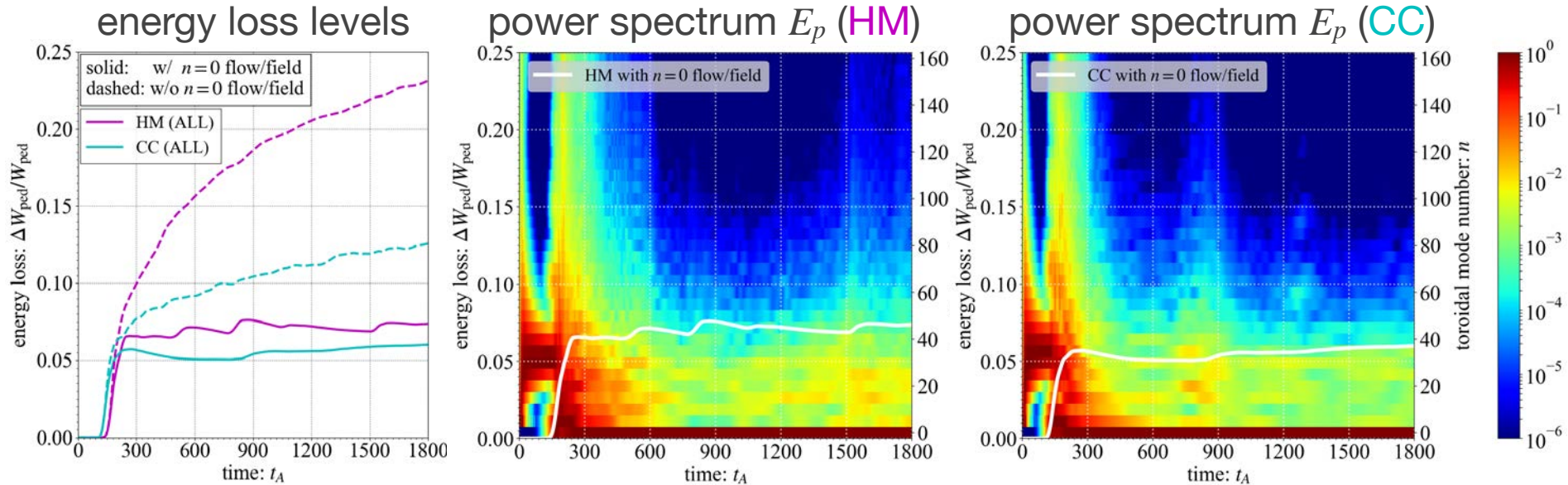
Impact of $n=0$ flow/field on Energy Loss



- $n=0$ flow/field have large impact on energy loss in both models
- Energy loss levels and power spectrum with $n=0$ flow/field show considerable difference between **HM** and **CC** models
 - ✓ Energy loss level oscillates after $t \sim 500t_A$ in **HM model**
 - ✓ Secondary crash is observed at $t \sim 800t_A$ in **CC model**

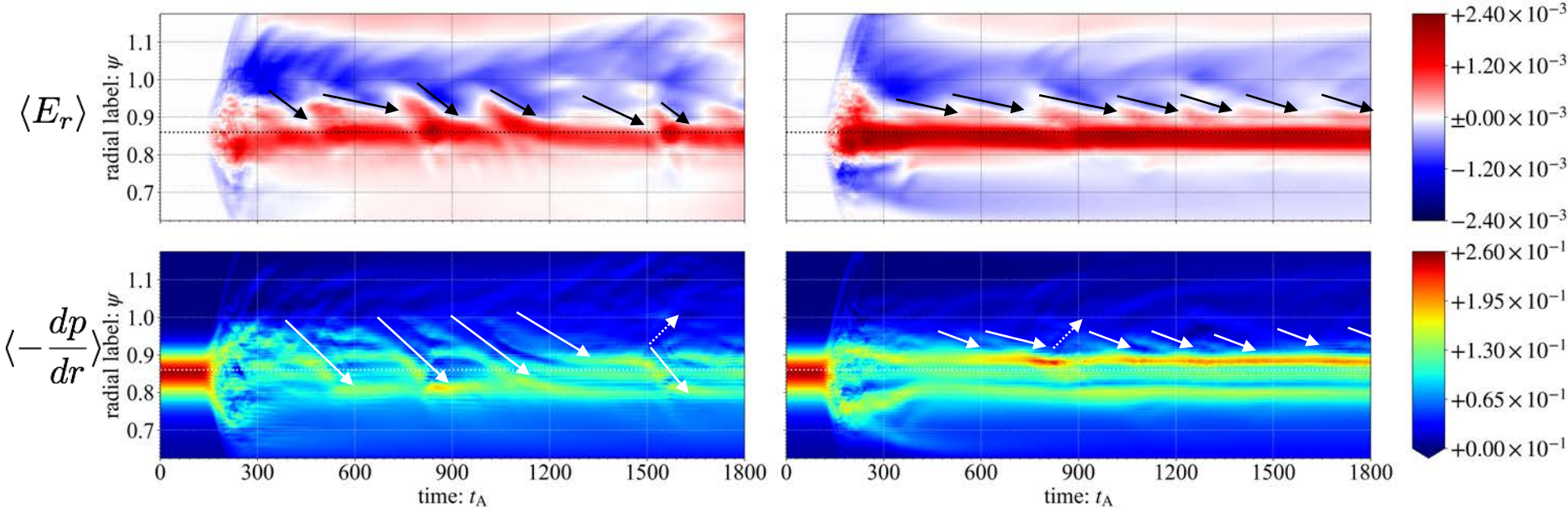
Note: energy loss is defined by released energy from $\psi=0.86$

Impact of $n=0$ flow/field on Energy Loss



- $n=0$ flow/field have large impact on energy loss in both models
- Energy loss levels and power spectrum with $n=0$ flow/field show considerable difference between **HM** and **CC** models
 - ✓ Energy loss level oscillates after $t \sim 500t_A$ in **HM** model
 - ✓ Secondary crash is observed at $t \sim 800t_A$ in **CC** model

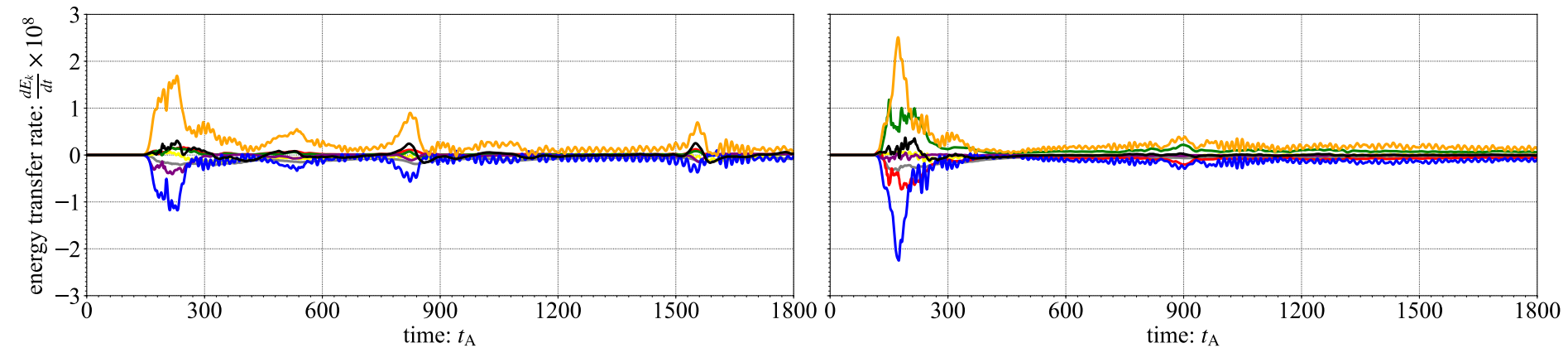
Note: energy loss is defined by released energy from $\psi=0.86$



Limit cycle oscillations (LCOs, solid arrows) are observed in $0.9 < \psi < 1.0$ after relaxation $t = 400t_A$ in both models but difference of E_r shear intensity gives qualitative difference

✓ Pressure gradient fronts by LCOs across $\psi = 0.86$ in **HM model**

✓ Strong E_r shear locks pressure gradient front at around $\psi = 0.90$ and triggers secondary collapse at $t = 800t_A$ pressure gradient front of which propagates outward (dashed arrow) in **CC model**



$$\frac{\partial E_k}{\partial t} = \underbrace{-\langle \phi_1 [\phi_1, U_1] \rangle_V}_{\text{green}} - \underbrace{\langle \phi_1 \mathcal{G}(p_0, \phi_1) \rangle_V - \langle \phi_1 \mathcal{G}(p_1, \phi_1) \rangle_V}_{\text{red}}$$

$$+ \underbrace{\langle \phi_1 \nabla_{\parallel 0} J_{\parallel 1} \rangle_V}_{\text{blue}} - \underbrace{\langle \phi_1 B_0 \left[A_{\parallel 1}, \frac{J_{\parallel 1}}{B_0} \right] \rangle_V}_{\text{purple}} - \underbrace{\langle \phi_1 B_0 \left[A_{\parallel 1}, \frac{J_{\parallel 0}}{B_0} \right] \rangle_V}_{\text{yellow}}$$

$$\underbrace{-\langle \phi_1 \mathcal{K}(p_1) \rangle_V}_{\text{orange}} - \underbrace{\langle \mu_{\parallel} |\partial_{\parallel 0} \phi_1|^2 \rangle_V}_{\text{grey}} - \underbrace{\langle \mu_{\perp} |\nabla_{\perp 0} \phi_1|^2 \rangle_V}_{\text{grey}}$$

$$\frac{\partial E_k}{\partial t} = \underbrace{-\langle F_1 [F_0, W_1] \rangle_V - \langle F_1 [F_1, W_0] \rangle_V - \langle F_1 [F_1, W_1] \rangle_V}_{\text{green}}$$

$$+ \underbrace{\langle F_1 \mathcal{G}(p_0, F_1) \rangle_V + \langle F_1 \mathcal{G}(p_1, F_0) \rangle_V + \langle F_1 \mathcal{G}(p_1, F_1) \rangle_V}_{\text{red}}$$

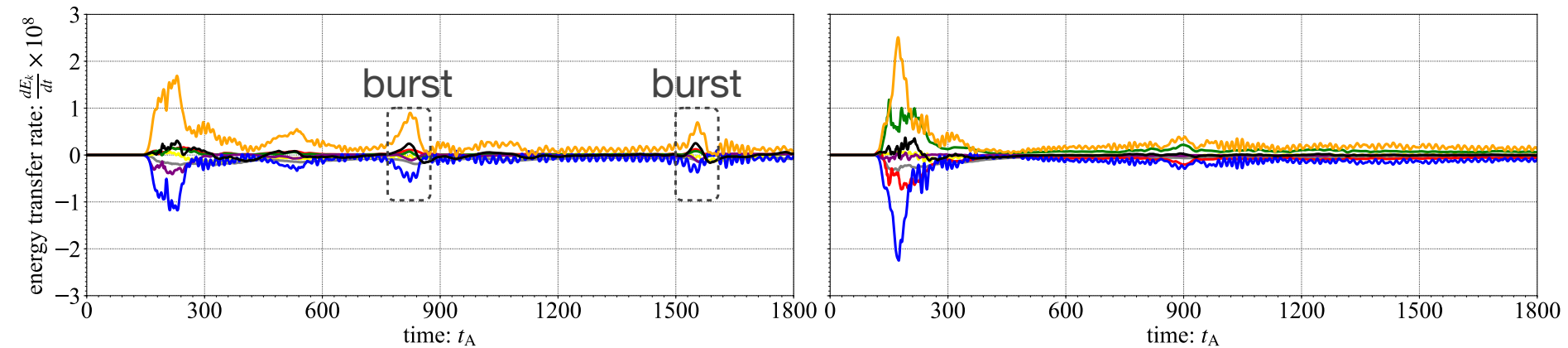
$$+ \underbrace{\langle F_1 \nabla_{\parallel 0} J_{\parallel 1} \rangle_V}_{\text{blue}} - \underbrace{\langle F_1 B_0 \left[A_{\parallel 1}, \frac{J_{\parallel 1}}{B_0} \right] \rangle_V}_{\text{purple}} - \underbrace{\langle F_1 B_0 \left[A_{\parallel 1}, \frac{J_{\parallel 0}}{B_0} \right] \rangle_V}_{\text{yellow}}$$

$$\underbrace{-\langle F_1 \mathcal{K}(p_1) \rangle_V}_{\text{orange}} - \underbrace{\langle \mu_{\parallel} |\partial_{\parallel 0} F_1|^2 \rangle_V}_{\text{grey}} - \underbrace{\langle \mu_{\perp} |\nabla_{\perp 0} F_1|^2 \rangle_V}_{\text{grey}}$$

- Contribution from **line-bending** and **curvature** are dominant
- $n=0$ flow generation mechanism in ELM crash differs from that of ITG turbulence (residual **Reynolds stress**)

$n=0$ flow/field (mean flow) are generated to recover force balance with pressure deformed by pedestal collapse

➔ Solving $n=0$ Ohm's law (update $n=0$ $J \times B$ force) is important.



$$\frac{\partial E_k}{\partial t} = \begin{aligned} & - \langle \phi_1 [\phi_1, U_1] \rangle_V \\ & - \langle \phi_1 \mathcal{G}(p_0, \phi_1) \rangle_V - \langle \phi_1 \mathcal{G}(p_1, \phi_1) \rangle_V \\ & + \langle \phi_1 \nabla_{\parallel 0} J_{\parallel 1} \rangle_V - \langle \phi_1 B_0 \left[A_{\parallel 1}, \frac{J_{\parallel 1}}{B_0} \right] \rangle_V - \langle \phi_1 B_0 \left[A_{\parallel 1}, \frac{J_{\parallel 0}}{B_0} \right] \rangle_V \\ & - \langle \phi_1 \mathcal{K}(p_1) \rangle_V - \langle \mu_{\parallel} |\partial_{\parallel 0} \phi_1|^2 \rangle_V - \langle \mu_{\perp} |\nabla_{\perp 0} \phi_1|^2 \rangle_V \end{aligned}$$

$$\frac{\partial E_k}{\partial t} = \begin{aligned} & - \langle F_1 [F_0, W_1] \rangle_V - \langle F_1 [F_1, W_0] \rangle_V - \langle F_1 [F_1, W_1] \rangle_V \\ & + \langle F_1 \mathcal{G}(p_0, F_1) \rangle_V + \langle F_1 \mathcal{G}(p_1, F_0) \rangle_V + \langle F_1 \mathcal{G}(p_1, F_1) \rangle_V \\ & + \langle F_1 \nabla_{\parallel 0} J_{\parallel 1} \rangle_V - \langle F_1 B_0 \left[A_{\parallel 1}, \frac{J_{\parallel 1}}{B_0} \right] \rangle_V - \langle F_1 B_0 \left[A_{\parallel 1}, \frac{J_{\parallel 0}}{B_0} \right] \rangle_V \\ & - \langle F_1 \mathcal{K}(p_1) \rangle_V - \langle \mu_{\parallel} |\partial_{\parallel 0} F_1|^2 \rangle_V - \langle \mu_{\perp} |\nabla_{\perp 0} F_1|^2 \rangle_V \end{aligned}$$

- Bursts occur in contributions from **line-bending** and **curvature** and energy transfer rate also temporally vary only in **HM model**
- Contributions from **Reynolds stress** and **ion diamag. stress** in **HM model** are smaller than those in **CC model**

These differences may result in qualitative difference of LCOs but further analyses are required to find out a key factor

1. Backgrounds and Motivations
2. Numerical Scheme for $n=0$ flow/field Driven by high- n Modes
3. Role of $n=0$ flow/field in ELM crash
4. Summary and Future Works

Summary

- **A numerical scheme for BOUT++ code to simulate ELM crash with $n=0$ flow/field has been proposed**
 - ✓ Poisson solver
 - ❖ Flute-ordered 1D-Helmholtz Eq. solver for resonant modes
 - ❖ **2D-Helmholtz Eq. solver for $n=0$ mode**
 - ✓ Poisson bracket
 - ❖ **Symmetric discretization scheme (z :FFT+ ψ y :4th central)**
- **The proposed scheme has been validated by HM 4-f model with multi-helicity initial perturbation in circular geometry**
 - ✓ Energy conservation and energy cascade/inverse cascade
 - ✓ Fine filament structures of flow/field during ELM crash
 - ✓ Global structures of $n=0$ flow/field after nonlinear relaxation

Summary and Future Works: 2/2

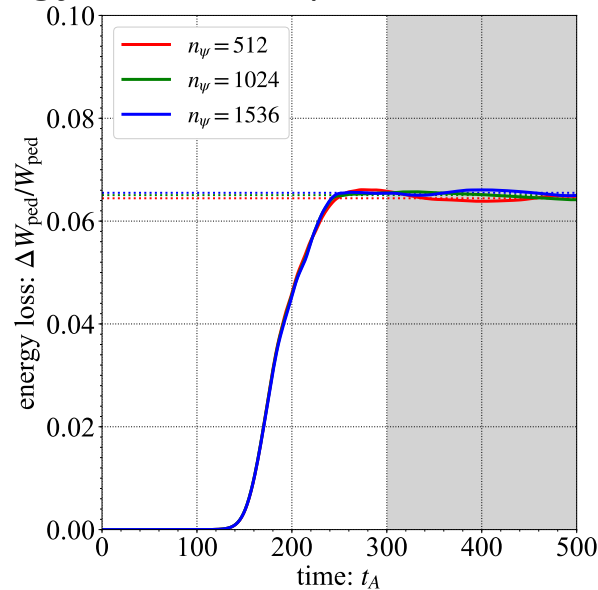
- **Role of $n=0$ flow/field on ELM crash process has been investigated with HM and CC model**
 - ✓ $n=0$ flow/field have large impact on energy loss in both models
 - ❖ **Convective cell shears pressure filaments**
 - ✓ LCOs are observed in both models but difference of E_r shear intensity gives qualitative difference
 - ❖ **Pressure gradient by LCOs goes to inner region in HM model**
 - ❖ **Pressure gradient are locked by strong E_r shear in CC model**
 - ✓ $n=0$ flow/field are generated to recover force balance rather than by residual Reynolds stress in both models

Future Works

- ✓ Improvement of physics models (5-/6-field w/ plasma rotation)
- ✓ ELM crash simulation with diverted geometries
- ✓ Development of 3D conservative scheme for Poisson bracket₁₇

Backup Slides

energy loss level (HM with $n=0$ flow/field)



- Maximum relative difference of saturated energy loss ($t > 300t_A$, sampling interval $\Delta t = 1t_A$) against that of $n_x = 1536$ is 1.8% ($n_x = 512$)
 ➔ $n_x = 512$ is fine enough to obtain saturated energy loss level
- This result supports that spectrum contamination in ELM crash with WENO scheme is triggered by numerical nonlinearity

To capture spikes of filaments during ELM crash, $n_x = 512$ is not fine enough and $n_x = 1024$ or finer is required

- HM model for IBM + ion diamag.

$$\frac{\partial U_1}{\partial t} = -\nabla_{\parallel 0} J_{\parallel 1} + B_0 \left[A_{\parallel 1}, \frac{J_{\parallel 0}}{B_0} \right] + \mathcal{K}(p_1) - \mathcal{G}(\phi_1, p_0)$$

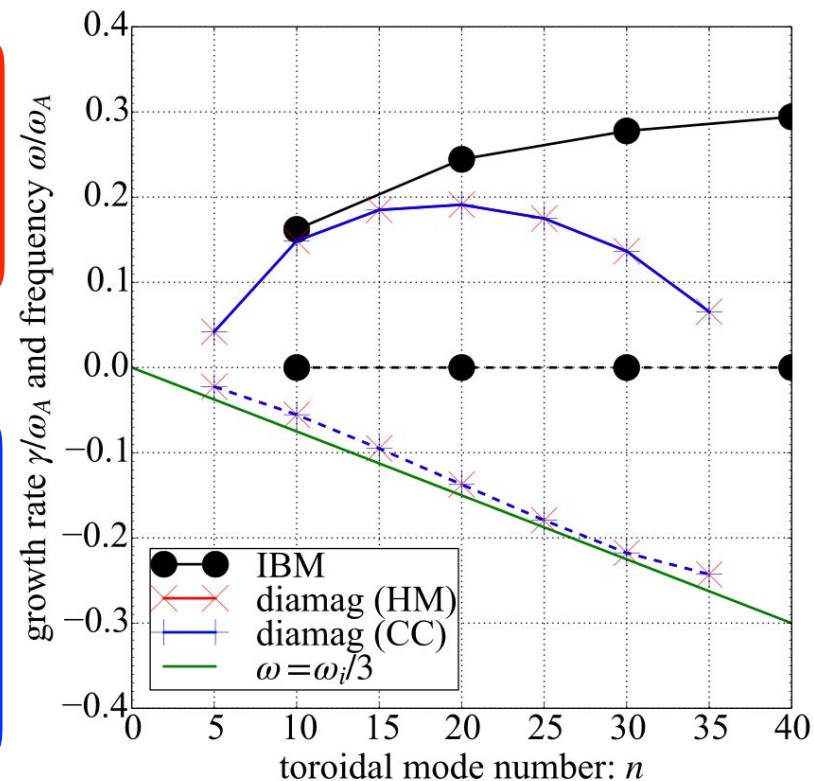
$$\frac{\partial p_1}{\partial t} = -[\phi_1, p_0], \quad \frac{\partial A_{\parallel 1}}{\partial t} = -\partial_{\parallel 0} \phi_1$$

- CC model for IBM + ion diamag.

$$\frac{\partial W_1}{\partial t} = -\nabla_{\parallel 0} J_{\parallel 1} + B_0 \left[A_{\parallel 1}, \frac{J_{\parallel 0}}{B_0} \right] + \mathcal{K}(p_1)$$

$$- [F_0, W_1] - [F_1, W_0] + \mathcal{G}(p_0, F_1) + \mathcal{G}(p_1, F_0)$$

$$\frac{\partial p_1}{\partial t} = -[\phi_1, p_0], \quad \frac{\partial A_{\parallel 1}}{\partial t} = -\partial_{\parallel 0} \phi_1$$



- $n=20$ IBM growth rate matches with Dudson+ CPC2009

✓ elm-4f: $\gamma = 0.244\omega_A$ ✓ elm_pb: $\gamma = 0.245\omega_A$ ✓ ELITE: $\gamma = 0.239\omega_A$

- Growth rates and rotating frequencies of HM and CC model shows good agreement as theoretically expected